High-Resolution Ion-Imaging Studies of the Photodissociation of the $BrCl^+$ Cation†

N. Hendrik Nahler, Olivier P. J. Vieuxmaire, Josephine R. Jones, and Michael N. R. Ashfold*

School of Chemistry, University of Bristol, Bristol, U.K., BS8 1TS

André T. J. B. Eppink

Department of Chemistry, University of Leeds, Leeds, U.K., LS2 9JT

A. Marcela Coriou and David H. Parker

University of Nijmegen, Department of Molecular and Laser Physics, Toernooiveld 1, 6525 ED, Nijmegen, The Netherlands

Received: February 19, 2004; In Final Form: May 4, 2004

The photofragmentation of state-selected $BrCl^+$ cations has been investigated by velocity-map ion-imaging methods. Detailed analyses of the $^{79}Br^+$ fragment velocities lead to the most precise values yet reported for (i) the spin−orbit coupling constant for the $X^2\Pi$ state, $A = -2070 \pm 4$ cm^{-1}; (ii) the bond dissociation energies of both states of $^{79}Br^{35}Cl^+$, 25019 ± 4 cm^{-1} ($X^2\Pi_{3/2}$) and 22949 ± 2 cm^{-1} ($X^2\Pi_{1/2}$); and (iii) the adiabatic ionization thresholds for forming $^{79}Br^{35}Cl^+$ parent ions in their $X^2\Pi_{3/2}$ and $X^2\Pi_{1/2}$ states, 88292 ± 6 and 90362 ± 4 cm^{-1}, respectively.

Introduction

Ion-imaging methods,[1] particularly the velocity-mapping variant of the technique,[2] are enabling new and detailed high-resolution investigations of the photodissociation[3−9] and photoionization[10,11] of a wide range of gas-phase molecules. The fragment of interest in almost all such studies reported thus far has been a neutral species, which is then ionized at source, with quantum state specificity, using an appropriate resonance-enhanced multiphoton ionization (REMPI) scheme and detected with a time- and position-sensitive detector. Analysis of the resulting image affords a direct visualization of the velocity (i.e., speed and angular) distribution of the probed product and, through energy and momentum conservation, of the undetected partner species.[12] More elaborate experiments, involving appropriate combinations of photolysis and/or REMPI probe laser propagation directions and polarizations can reveal higher moments of the recoil distribution, e.g., the orientation and/or alignment of one or more of the products.[4−6,13,14]

The past year has witnessed a number of reports of the application of velocity-map imaging methods to studies of the photofragmentation of molecular ions, e.g., Br_2^+ (refs 15 and 16) and CF_3I^+ (ref 17). The precursor in such experiments is a state-selected molecular ion, $BrCl^+$ in the present work, which is created in a defined electronic, spin−orbit, and vibrational state by REMPI. Photodissociation of the molecular ion so formed yields an ionic fragment (here Br^+ or Cl^+), which can be imaged directly. The $BrCl^+$ cation has an inverted $^2\Pi$ ground state derived from the electronic configuration ...$(12\sigma)^2(5\pi)^4(6\pi)^3(13\sigma)^0$. The available thermochemical and spectroscopic information relating to this ion still relies heavily on the analysis of the early He I photoelectron spectrum of Dyke and coworkers,[18] which suggested a vertical ionization potential (IP) for forming ground-state ($^2\Pi_{3/2}$) ions of 11.012 ± 0.005 eV (88820 ± 40 cm^{-1}), a ground-state spin−orbit splitting of 2070 ± 30 cm^{-1}, and an estimated bond-dissociation energy, D_e = 25400 ± 80 cm^{-1} for the $^2\Pi_{3/2}$ state of the cation.

The type of study described in this work requires use of REMPI methods to prepare the state-selected molecular ion. There appear to be no published REMPI spectra of BrCl. Though the visible and near-ultraviolet absorption spectrum of BrCl has been investigated in some detail,[9,19] our knowledge of the higher-lying excited states of this molecule is limited. Vacuum ultraviolet absorption spectroscopy has revealed two short vibronic progressions in the wavelength range 155−170 nm, labeled $b_5 \leftarrow X$ and $a_5 \leftarrow X$, which have been assigned to the first ($n = 5$) member of the $ns\sigma \leftarrow 6\pi$ Rydberg series, split by the spin−orbit splitting of the $^2\Pi$ ion core.[20] Absorption observed during excitation at shorter wavelengths, in the range 144−155 nm, has been attributed to population of, predominantly, the ion pair state labeled E, with $\Omega = 0^+$. Further characterization of the E 0^+ state has been provided by analyses of its wavelength-resolved emission (which deduced that the E state potential minimum lies at $R_e \approx 3.042$ Å and an energy of ~48760 cm^{-1} and that the E state well depth $D_e \approx 35\,780$ cm^{-1} (ref 21)) and, at much higher resolution, of portions of the rovibrationally resolved E $0^+ \leftarrow$ X 0^+ absorption spectrum.[22] The large, wavelength-dependent variations in vibronic band intensity observed in this latter study were attributed to perturbations with other excited states arising from, for example, the $5p \leftarrow 6\pi$ Rydberg excitations.

Here we report the first high-resolution imaging studies of (i) the photoelectrons arising in the multiphoton ionization of BrCl, resonance enhanced at the two photon energy by the $v' = 0$ level of the $[^2\Pi_{1/2}]5s\sigma$ Rydberg state, (ii) the Br^+ fragment

† Part of the special issue "Richard Bersohn Memorial Issue".

* To whom correspondence may be addressed. Tel.: 0117-9288312/3. Fax: 0117-9250612. E-mail:mike.ashfold@bris.ac.uk.

10.1021/jp049238q CCC: $27.50
Published on Web 06/11/2004

ions arising in one-color REMPI of BrCl at various wavelengths in the range $310 \leq \lambda_{prep} \leq 340$ nm (chosen so as to be resonant, at the two-photon energy, with levels observed in the $b_5 \leftarrow X$ and $a_5 \leftarrow X$ progressions), and (iii) the Br^+ fragment ions that arise when state-selected $BrCl^+$ ions prepared by $2 + 1$ REMPI are photolyzed at wavelengths in the range $370 \leq \lambda_{phot} \leq 436$ nm. Analysis yields much refined values for the ionization energy of ground-state BrCl molecules, the dissociation energies of $BrCl^+$ ions in both their $X^2\Pi_{3/2}$ and $X^2\Pi_{1/2}$ spin−orbit states, and the spin−orbit splitting in the $X^2\Pi$ state. The study provides further graphic illustration of the new opportunities offered by high-resolution imaging methods in studies of the photofragmentation of state selected molecular ions.

Experimental Section

The photoelectron and ion-imaging studies reported herein were conducted in Nijmegen and Bristol, respectively. Both apparatus have been described in detail previously.[3,23] Both experiments employed a pulsed, skimmed, supersonic beam containing BrCl molecules (in equilibrium in a mixture comprising 25 Torr Br_2 and 150 Torr Cl_2, made up to a total pressure of 1 atm in Ar) directed at the center of the detector (i.e., along the *Z* axis). The skimmed beam in both experiments was crossed at right angles by the output of one (or two) pulsed tunable dye lasers which (counter)propagate along the *X* axis. The Nijmegen experiment involved a single Nd:YAG pumped dye laser (Continuum Surelite plus Radiant Dye Narrowscan), the output of which was frequency doubled to generate pulses of linearly polarized (ϵ // *Y*) UV radiation (500 μJ pulse^{-1}, 10 Hz repetition rate) at wavelengths appropriate for two-photon resonant MPI via selected levels of the $[^2\Pi]5s\sigma$ Rydberg state and focused (20-cm focal length lens) into the interaction volume. The resulting photoelectrons were extracted, along *Z*, under velocity map imaging conditions. The electron cloud impinged on the front face, 350 mm downstream from the interaction volume, of a position-sensitive detection system comprising of a pair of microchannel plates and a phosphor screen, which was viewed by a CCD camera running in the event counting mode. Given the rather high background photoelectron signal arising as a result of UV photoionization of gas-phase species present in the base vacuum of this spectrometer, it was necessary to record two photoelectron images recorded under identical operating conditions, one with the molecular beam on, the other with it off, and to analyze the difference between the "beam on" and "beam off" images.

Ion-imaging studies in Bristol employed two tunable lasers. Laser 1, an Nd:YAG pumped frequency-doubled dye laser (Spectra-Physics GCR-250 plus Sirah Cobra Stretch, yielding an output bandwidth < 0.1 cm^{-1} in the visible), was used for one-color REMPI of BrCl molecules at a range of wavelengths λ_{prep} chosen so as to be two-photon resonant with different vibronic levels associated with the a_5 and b_5 systems. Inclusion of a Pockel's cell within the UV beam path allowed investigation of the sensitivity of the $BrCl^+$ parent and Br^+ fragment ion yields to the polarization state (linear or circular) of the REMPI laser radiation.[5] As shown below, one-color excitation at most of these wavelengths yielded large fragment ion signals; $BrCl^+$ parent ions made a substantial contribution to the total ion yield only in the case of excitation via the b_5, $v' = 0$ level. Most fragment ion-imaging experiments were therefore conducted at $\lambda_{phot} = 324.51$ nm (30 807.6 cm^{-1}), with ϵ_{prep} perpendicular to the molecular beam axis and parallel to the plane of the detector (i.e., ϵ_{prep} // *Y*). Wavelengths (in air) and the corresponding vacuum wavenumbers of all photons used in Bristol were measured using a wavemeter (Coherent, WaveMaster). The resulting $BrCl^+$ ions were photolyzed with the output of laser 2, a second tunable laser system (Spectra-Physics GCR-170 plus PDL-2 dye laser), which provided linearly polarized radiation in the wavelength range $370 < \lambda_{phot} < 436$ nm, with ϵ_{phot} // *Y*. Typical pulse energies used in the present work were 250−400 and 150−400 μJ for lasers 1 and 2, respectively. Both pulses were focused (20-cm focal length lenses) into the interaction region, monitored by a fast photodiode, and timed so that the laser pulse used to induce ion fragmentation was delayed by ~5 ns relative to the $BrCl^+$ ion-preparation pulse. As in our previous study of state-selected Br_2^+ ion photolysis,[16] the resulting ions were extracted, along *Z*, under velocity-map imaging conditions. The ion cloud impinges on the front face of a position-sensitive detector (again a pair of microchannel plates and a phosphor screen) located 860 mm downstream from the interaction volume, which is read out by a CCD camera equipped with a fast intensifier (Photonic Science) that is gated to the time-of-flight (TOF) of $^{79}Br^+$ (and/or $^{35}Cl^+$) ions. Each ion image resulting from a single laser shot was processed with an event-counting, centroiding algorithm provided with the commercial camera software DaVis (LaVision) running on a PC, and the resulting counts accumulated for, typically, 10^4 laser shots. Analysis of both the accumulated photoelectron and ion images involved reconstruction of the 3-D velocity distribution as described previously[24] using an algorithm based on the filtered back projection method of Sato et al.[25]

Results and Discussion

Several factors can aid (or hinder) the use of imaging methods for investigating the photofragmentation dynamics of molecular ions.[16] Apart from good spectrometer design, the use of event-counting methods for image collection, and accurate image-processing strategies, one of the most important is the degree of state selectivity achieved in the ion-preparation step. Some state selectivity can usually be achieved if the one- and/or multiphoton excitation spectra of the neutral precursor show a well-resolved Rydberg vibronic structure. This is important if, for example, as here, it is proposed to use one-color $2 + 1$ REMPI to prepare the parent ion and to rely on the well-documented propensity for core-conserving $\Delta v = 0$ transitions from the intermediate Rydberg level to ensure that these ions are formed, predominantly, in a single, well-defined, electronic, spin−orbit, and vibrational state.[26] However, the literature also contains numerous examples that show substantial fragment ion formation accompanying the parent REMPI process.[27] Such fragmentation can arise in various different ways. Fragment ion formation is almost inevitable if λ_{prep} is accidentally resonant with an electronic transition of the parent ion and the electronically excited ions so formed are dissociative (or predissociative). Fragment ions can also arise when the resonance-enhancing state of the neutral molecule is of mixed Rydberg, valence, and/or ion-pair character. Further photon absorption can lead to "super-excited" states lying at energies above the first ionization limit. These can ionize directly or indirectly (autoionize). They can also dissociate, to ionic and neutral fragments, or yield neutral fragments, one (or more) of which are electronically excited. Further photon absorption by such electronically excited neutral photofragments is yet another route to forming fragment ions.[28] Any such mechanism whereby fragment ions are formed as a by-product of the parent REMPI process at wavelength λ_{prep} will hamper observation of the fragment ion signal of interest induced by λ_{phot} and degrade the signal-to-noise ratio of the required two-color fragment ion images.

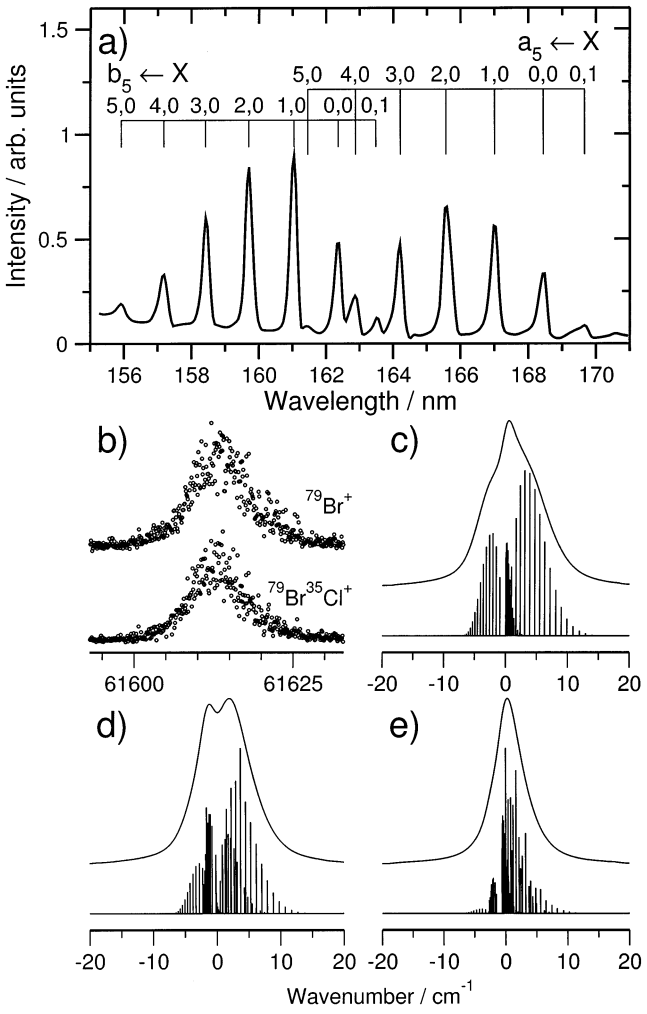

Figure 1. (a) One-photon absorption spectrum of BrCl recorded in the wavelength range $155 < \lambda < 171$ nm (after ref 20), with vibronic features associated with the $a_5 \leftarrow X$ and $b_5 \leftarrow X$ transitions indicated. (b) Excitation spectra for forming $^{79}Br^{35}Cl^+$ and $^{79}Br^+$ ions via MPI, resonance enhanced at the two-photon energy by the $v' = 0$ level of the b_5 state. Simulated band contour simulations of the three possible second-rank components of the two-photon transition tensor (T_0^2(A), T_1^2(A), and T_2^2(A)) are shown in panels c−e, respectively. Each of these simulations assumes $B_0'' = 0.15285$ cm^{-1}, $B' = 0.1655$ cm^{-1}, a transition band origin at 0 cm^{-1}, $T_{rot} = 8$ K, and values of 0.1 cm^{-1} (stick spectrum) and 3 cm^{-1} (overlying envelope, offset vertically for clarity), respectively, for the fwhm line widths of the individual rovibronic transitions.

One Color Studies. For orientation, Figure 1a reproduces the relevant part of the one-photon absorption spectrum of BrCl reported previously.[20] Ion TOF spectra were recorded following excitation of a jet-cooled Br_2/Cl_2 equilibrium mixture at various λ_{prep} wavelengths chosen so as to be resonant, at the two-photon energy, with each of the $v' = 0-5$ vibronic levels of both the a_5 and b_5 states of BrCl. Four illustrative spectra are shown in Figure 2, following conversion from TOF to mass (m/z). The doublet appearing at TOFs appropriate for ions with mass to charge (m/z) ratios of 79 and 81, associated with $^{79}Br^+$ and $^{81}Br^+$ fragment ions, dominate each spectrum, but the relative yields of parent and fragment ions are seen to vary markedly with wavelength and/or resonant intermediate level. Indeed, only in the spectrum recorded at $\lambda_{prep} = 324.51$ nm ($\bar{\nu}_{prep} = 30\,807.6$ cm^{-1}) do peaks at $m/z = 114$, 116, and 118 (attributable to $BrCl^+$ parent ions) make a substantial contribution to the total ion yield. Br_2^+ parent ions are also evident in the ion TOF spectra, most notably at $\bar{\nu}_{prep} = 30\,458.0$ cm^{-1}, a wavenumber

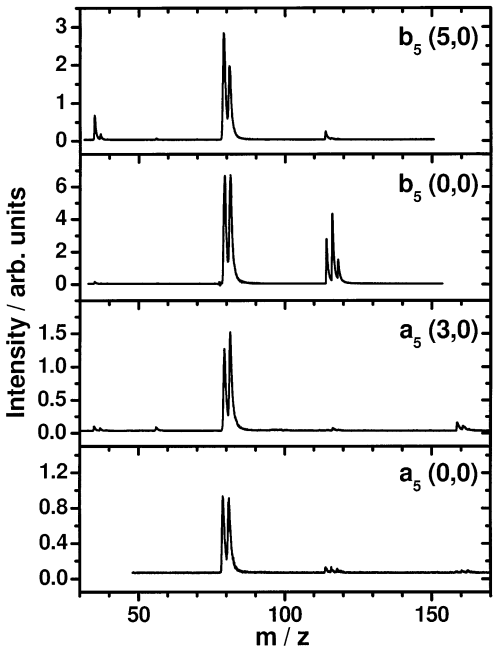

Figure 2. Ion mass spectra obtained following excitation at (from bottom to top): $\bar{\nu}_{prep} = 29\,701$ cm^{-1} (two-photon resonant with the $a_5 \leftarrow X$, (0,0) transition); 30 458 cm^{-1} ($a_5 \leftarrow X$, (3,0)); 30 807 cm^{-1} ($b_5 \leftarrow X$, (0,0)); 32 075 cm^{-1} ($b_5 \leftarrow X$, (5,0)).

that is accidentally two-photon resonant with both the $a_5 \leftarrow X$ (3,0) band of BrCl and with the $[^1/_2]5s;1_g \leftarrow X$ ($v' = 4 \leftarrow v'' = 0$) transition of Br_2.[29] Cl^+ fragment ions can be seen also, most notably in the TOF spectrum recorded at $\bar{\nu}_{prep} = 32\,075$ cm^{-1}.

Figure 1b also shows excitation spectra for forming $^{79}Br^{35}Cl^+$ and $^{79}Br^+$ ions via MPI, resonance enhanced at the two-photon energy by the $v' = 0$ level of the b_5 state. We believe these to be the first reported REMPI spectra of BrCl. Polarization-dependent studies at $\lambda_{prep} = 324.51$ nm (i.e., appropriate for REMPI via the b_5, $v' = 0$ level) showed that the ion signal increased (by a factor of nearly 2) on changing from linear- to circular-polarized excitation (while maintaining a constant laser intensity). Such an increase is characteristic of a multiphoton transition in which the least-probable step is carried by a second-rank component of the two-photon transition tensor, for which a 1.5× increase in transition probability would be predicted upon such a change of polarization.[26] Band contour simulations of the three possible second-rank components (T_0^2(A), T_1^2(A), and T_2^2(A)) that assume plausible values for the rotational temperature (T_{rot}) of the BrCl parent molecules, excited-state rotational constants, and transition line widths yield the envelopes shown in panels (c)−(e) in Figure 1. The ground-state rotational constant for $^{79}Br^{35}Cl$, $B_0'' = 0.15285$ cm^{-1} is well established.[30] Franck−Condon arguments[18] and analogy with Br_2[16] would suggest a reduction in equilibrium bond length and thus an increase in the B value upon $b_5 \leftarrow X$ excitation. Our choice of $B' = 0.1655$ cm^{-1} for the Rydberg excited state is guided by the results of preliminary ab initio calculations of the ground state (and excited valence states) of $BrCl^+$.[31] The assumed value for T_{rot} (~8 K) follows from our previous studies of Br_2 in this same spectrometer.[15] Previous analyses have associated the b_5-X (and a_5-X) systems with the spin−orbit split $5s\sigma \leftarrow 6\pi$ ($\Omega' = 1 \leftarrow \Omega'' = 0$) transition, mainly on the basis of quantum defect considerations.[20] Such an assignment is generally consistent with the present band contour calculations, which assume a Lorentzian line width of ~3 cm^{-1} (full width half-maximum (fwhm)) for each rovibronic transition, though the apparent diffuseness of the measured spectrum precludes detailed spec-

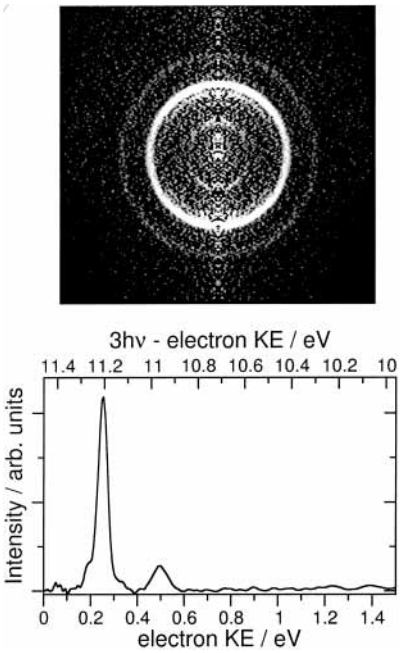

Figure 3. 2-D slice through the reconstructed 3-D velocity distribution derived by back projecting the (background subtracted and symmetrized) photoelectron image measured at $\bar{\nu}_{prep} = 30\,807.6$ cm^{-1}, along with the photoelectron speed distribution obtained by integrating over all angles after reconstruction of the 3-D velocity distribution.

troscopic analysis. The 3-cm^{-1} line width assumed, which is more than an order of magnitude greater than the effective two photon bandwidth of the exciting laser radiation, is most readily explained as being due to the short (~1.7 ps) lifetime of the predissociated b_5 level. Such efficient homogeneous broadening, allied with the more dense rovibronic structure accompanying the T_1^2(A) component of the two-photon transition moment, must result in a much poorer rotational-state specificity in the parent ion preparation step than was the case in our recent studies of Br_2^+.[15] Clearly, dissociation at the energy of one absorbed photon[9] and predissociation at the two-photon energy will both serve to reduce the efficiency of $BrCl^+$ ion formation by three-photon ionization at these excitation wavelengths.

The aim of the present work was to study the photofragmentation of state-selected $BrCl^+$ parent ions. Given the extent of the observed fragment ion formation, it was deemed prudent to measure the kinetic energies of the accompanying photoelectrons in order to establish more clearly the fragment ion formation routes. Photoelectron images were thus recorded at a number of wavelengths corresponding (at the two-photon energy) with various $a_5 \leftarrow X$ and $b_5 \leftarrow X$ vibronic band maxima. Figure 3 shows a 2-D slice through the reconstructed 3-D velocity distribution derived by back projecting the (background subtracted and symmetrized) image measured at $\bar{\nu}_{prep} = 30\,807.6$ cm^{-1} − the wavenumber of the $b_5 \leftarrow X$ (0,0) transition, at which the $BrCl^+$ parent ion peak is largest. The necessary pixel → velocity calibration factor was obtained by imaging photoelectrons, using the same extraction voltages, from two systems for which the ionization energies are well-documented: REMPI of Br_2 at $\bar{\nu}_{prep} = 29\,717$ cm^{-1} (resonance enhanced at the two-photon energy by the $[^1/_2]5s;1_g \leftarrow X$ origin band)[29] and of atomic Cl photofragments at $\bar{\nu}_{prep} = 30\,635.6$ and $30\,867.6$ cm^{-1}. In both of these latter cases, the documented resonance enhancement is at the three-photon energy.[32] The photoelectron speed distribution obtained by integrating over all angles after reconstructing the 3-D velocity distribution (also shown in Figure 3) shows a dominant peak at a photoelectron kinetic

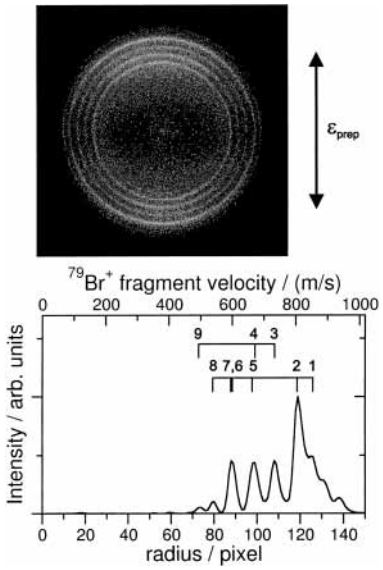

Figure 4. Raw image of $^{79}Br^+$ ions recorded following excitation at $\bar{\nu}_{prep} = 30\,807.6$ cm^{-1}, with ϵ_{prep} aligned vertically in the displayed image, together with the associated speed distribution obtained by integrating over all angles after reconstruction of the 3-D velocity distribution. The comb superimposed above the speed distribution indicates the various parent → product channels as defined in Table 1.

energy, E_e ~0.25 eV, and a weaker feature at E_e ~0.49 eV. As we show below, the subsequent ion-image analysis will validate what, at this stage, seems the most plausible interpretation of this spectrum, namely, that the cations formed in association with the measured photoelectrons are indeed $BrCl^+$, in the $v^+ = 0$ levels of the excited ($^2\Pi_{1/2}$) and ground ($^2\Pi_{3/2}$) spin−orbit states, respectively. The respective peak areas imply that ~84% of the parent ions formed via 2 + 1 REMPI at $\bar{\nu}_{prep} = 30\,807.6$ cm^{-1} are in the $^2\Pi_{1/2}$ spin−orbit state. The shoulder on the low kinetic energy side of the large peak is consistent with a small yield of $BrCl^+(^2\Pi_{1/2})$, $v^+ = 1$ ions. The respective ionization potentials so derived, which can be read off the top axis of Figure 3, are in good accord with the values reported by Dunlavey et al.[18] These will be defined more precisely from the subsequent analyses of fragment ion images.

Given the simplicity of this photoelectron image and its interpretation and the absence of any additional rings attributable to photoionization of neutral Br atoms, it follows that most if not all of the observed Br^+ fragment ions must arise via the process that is the focus of this work, namely, the one (or more) photon excitation of $BrCl^+$ cations. Such is consistent with the observed similarity of the excitation spectra for forming $BrCl^+$ and Br^+ ions shown in Figure 1b. Figure 4 shows a one-color image of $^{79}Br^+$ ions recorded following excitation at $\bar{\nu}_{prep} = 30\,807.6$ cm^{-1}, with ϵ_{prep} // Y (i.e., vertical in the image as displayed). The image reveals a number of concentric rings, corresponding to various different $BrCl^+(^2\Pi_\Omega) \rightarrow Br^+(^3P_J) + Cl(^2P_J)$ fragmentations, all of which show a preference for recoil parallel to ϵ_{prep}. The speed distribution obtained by integrating over all angles after reconstruction of the 3-D velocity distribution is shown in the accompanying panel. To simplify the ensuing discussion, Table 1 lists the 12 lowest-energy parent → product correlations that might contribute to this and subsequent images presented in this work in terms of just two unknowns, $D_0(Br^+-Cl)$, here defined as the dissociation energy of $BrCl^+(^2\Pi_{1/2})$ ions in their $v^+ = 0$ state, and $|A|$, the magnitude of the spin−orbit splitting in the ground state of $BrCl^+$. The energetic ordering of the various thresholds is already clear, given the approximate value of $|A|$ obtained from the present

TABLE 1: First 12 Fragmentation Channels of $BrCl^+(^2\Pi_{\Omega=1/2,3/2})$ Cations, in Their Respective $v^+ = 0$ Levels, Listed in Order of Increasing Threshold Energy[a]

channel no.	Ω state of $BrCl^+$	J state of $Br^+(^3P)$	J state of $Cl(^2P)$	threshold energy/cm^{-1}
1	1/2	2	3/2	$D_0(Br^+-Cl)$
2	1/2	2	1/2	$D_0(Br^+-Cl) + 882.4$
3	3/2	2	3/2	$D_0(Br^+-Cl) + \|A\|$
4	3/2	2	1/2	$D_0(Br^+-Cl) + \|A\| + 882.4$
5	1/2	1	3/2	$D_0(Br^+-Cl) + 3136.4$
6	1/2	0	3/2	$D_0(Br^+-Cl) + 3837.5$
7	1/2	1	1/2	$D_0(Br^+-Cl) + 4018.8$
8	1/2	0	1/2	$D_0(Br^+-Cl) + 4719.9$
9	3/2	1	3/2	$D_0(Br^+-Cl) + \|A\| + 3136.4$
10	3/2	0	3/2	$D_0(Br^+-Cl) + \|A\| + 3837.5$
11	3/2	1	1/2	$D_0(Br^+-Cl) + \|A\| + 4018.8$
12	3/2	0	1/2	$D_0(Br^+-Cl) + \|A\| + 4719.9$

[a] For the purpose of this table, $D_0(Br^+-Cl)$ represents the dissociation energy of $BrCl^+(^2\Pi_{\Omega=1/2})$ ions in their ground vibrational state, and $|A|$ is the magnitude of the spin−orbit splitting in the $^2\Pi$ ground state of $BrCl^+$, both of which are derived in the present analysis.

and earlier[18] photoelectron measurements and the well-documented spin−orbit splittings in the Br^+ and Cl products (Br^+, $E(^3P_2) = 0$ cm^{-1}, $E(^3P_1) = 3136.4$ cm^{-1}, $E(^3P_0) = 3837.5$ cm^{-1}; Cl, $E(^2P_{3/2}) = 0$ cm^{-1}, $E(^2P_{1/2}) = 882.4$ cm^{-1}).[33] The comb superimposed above the speed distribution in Figure 4 indicates that 324.51-nm photolysis of the distribution of $BrCl^+$ ions formed by $2 + 1$ REMPI at this same wavelength leads to some activity in most if not all of the nine lowest-energy fragmentation channels. The additional unlabeled structure evident at largest radius is attributable to fragmentation of the small fraction of vibrationally excited $BrCl^+(^2\Pi_{1/2})$ ions formed in the REMPI preparation step. The relative intensities of the peaks associated with channels 1 and 2 in Figure 4 indicate that, at this wavelength, $BrCl^+(^2\Pi_{1/2})$ ions dissociate preferentially to ground-state Br^+ and spin−orbit excited Cl atoms. The limited energy resolution of this one-color image, coupled with the near degeneracy of channels 4 and 5, prevents us making any similarly detailed comment about the relative probabilities of forming ground and spin−orbit excited Cl atoms from $BrCl^+(^2\Pi_{3/2})$ photolysis at this wavelength.

Two Color Studies. In our previous studies of Br_2^+ photolysis,[15,16] it was possible to find λ_{prep} and λ_{phot} combinations and relative pulse energies such that the two-color signal was significantly larger than that induced by λ_{prep} alone. Subtracting one from the other yielded "two-color-only" images, which could be analyzed to yield detailed spectroscopic and thermochemical data for the parent ion, and details concerning its primary photofragmentation dynamics. As Figure 2 showed, Br^+ fragment ions dominate the ion yield from $2 + 1$ REMPI of BrCl at all wavelengths in the range $310 \le \lambda_{prep} \le 340$ nm. Fortunately, however, all of the Br^+ ions so formed have recoil velocities $v > 500$ m s^{-1}. The central parts of the one-color images are relatively clean. Any Br^+ ions arising from photolysis of $BrCl^+$ at energies close above the lowest dissociation threshold(s) will be formed with low kinetic energy and thus appear in this "empty" center part of the image.

This thinking underlies all of the two-color studies reported in the remainder of this work. The vast majority of such studies involved excitation at the peak of the $b_5 \leftarrow X$ (0,0) resonance at $\bar{\nu}_{prep} = 30\,807.6$ cm^{-1} and monitoring of the $^{79}Br^+$ fragment ion. This excitation wavelength was chosen because it offers the greatest parent/fragment ion ratio, but it suffers the disadvantage (relative to use of a higher v' intermediate level) that it precludes discrimination in favor of ^{35}Cl or ^{37}Cl co-fragments. The left-hand column in Figure 5 shows four such

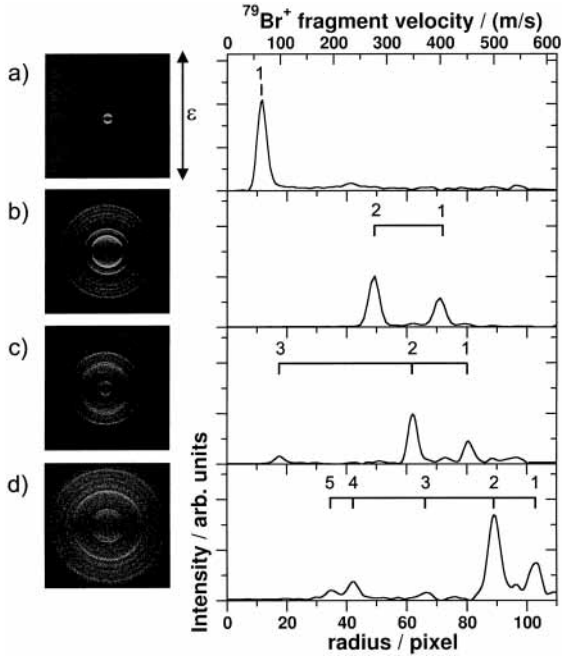

Figure 5. Raw images of $^{79}Br^+$ ions recorded following REMPI preparation of $BrCl^+$ parent ions at $\bar{\nu}_{prep} = 30\,807.6$ cm^{-1} and subsequent excitation at $\bar{\nu}_{phot} =$ (a) 23 000, (b) 24 650, (c) 25 126, and (d) 26 150 cm^{-1}, with ϵ_{prep} and ϵ_{phot} both aligned vertically as shown. Each image contains a one-color contribution at a large radius, most evident in panels (b) and (d). The associated speed distributions of the slow ($v < 600$ m s^{-1}) Br^+ fragments are shown on the right, with peaks associated with the various active parent → product channels labeled as in Table 1.

images recorded at $\bar{\nu}_{phot} = 23\,000$, 24 650, 25 126, and 26 150 cm^{-1}; the one-color contribution is present at a large radius in each of these images, though not necessarily evident with the gray scale used in their display. The associated speed distributions of the slow ($v < 600$ m s^{-1}) Br^+ fragments are shown on the right. The image recorded at $\bar{\nu}_{phot} = 23\,000$ cm^{-1} shows a single two-color ring, arising from $BrCl^+(^2\Pi_{1/2})$, $v^+ = 0$ ions dissociating via channel 1. This ring expands with increasing photon energy, and additional peaks appear as $\bar{\nu}_{phot}$ is increased. By $\bar{\nu}_{phot} = 26\,150$ cm^{-1}, peaks attributable to fragmentation processes 1−5 are all clearly recognizable.

As mentioned previously,[15,24] analysis of many such speed distributions, and their variation with $\bar{\nu}_{phot}$, allows derivation of a precise value for the bond dissociation energy of the $BrCl^+$ cation. The measured velocity distributions are fit to a function of the form

$$S(r) = \left(\frac{8 \ln 2}{\pi}\right)^{1/2} \left\{ \sum_{i=1}^{5} \left(\frac{S_i}{w_{1/2}} \exp[-4 \ln 2((r - r_i)/w_{1/2})^2] \right) \right\} \quad (1)$$

where i labels the various $BrCl^+(^2\Pi_\Omega) \rightarrow Br^+(^3P_J) + Cl(^2P_J)$ channels of interest (as defined in Table 1), S_i is the corresponding peak intensity, r_i is the radius in pixels, and $w_{1/2}$ is the width (fwhm) of the Gaussian function used to describe the velocity distribution associated with each of these fragmentation channels. r_i is related to the Br^+ fragment recoil velocity according to

$$r_i(\alpha, D_i) = \frac{1}{\alpha} \left[\frac{2 m_{Cl}(h\nu - D_i)}{m_{Br} m_T} \right]^{1/2} \quad (2)$$

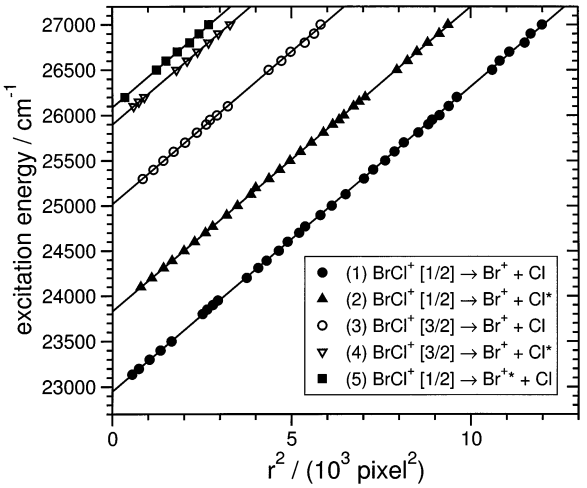

Figure 6. Plot of excitation energy vs squared best-fit image radius r^2 (in pixels squared, proportional to the kinetic energy) for $^{79}Br^+$ products arising from photodissociation of state-selected $BrCl^+$ ions via processes 1−5 as defined in the inset and in Table 1. Threshold energies for the different fragmentation channels, deduced via linear fitting of the respective data sets, are listed in Table 2.

TABLE 2: Effective Dissociation Thresholds, D_i, and Their 1σ Errors, Obtained from the Linear Fits to the Data Displayed in Figure 6

channel no., *i*	D_i/cm^{-1}
1	22 949.5 ± 1
2	23 831.3 ± 1
3	25 020.4 ± 3
4	25 900.2 ± 3
5	26 086.6 ± 3

where α is the proportionality constant linking the fragment recoil velocity and the image radius, $m_{Br} = 78.918$ amu, $m_{Cl} = 35.534$ amu, $m_T = (m_{Br} + m_{Cl})$, and D_i is the dissociation energy of the particular parent → product fragmentation process as defined in the last column of Table 1. As before, the fits were performed using the nonlinear Levenberg−Marquardt method.[34] As pointed out previously,[24] the correlation between α and D_i in eq 2 can be avoided, and α determined independently, in any image that shows products from two channels whose D_i values differ simply by the spin−orbit splitting of an atomic product. For example, given $E(^2P_{1/2}) = 882.4$ cm^{-1}, energy and momentum conservation allows us to determine

$$\alpha = \sqrt{\frac{2m_{Cl}E(^2P_{1/2})}{m_{Br}m_T(r_1^2 - r_2^2)}} \qquad (3)$$

from analysis of rings associated with channels 1 and 2 or 3 and 4. The fitting returns r values for the maxima of the various peaks in each velocity distribution, with subpixel resolution. The dissociation energies, D_i, can then be determined from the y-axis intercepts of linear fits to plots of photon energy vs the square of the corresponding r_i values as illustrated in Figure 6. The evident linearity and parallelism of these various plots is testimony to the apparatus design and the constancy of the α parameter (for a given set of ion extraction voltages).

Table 2 lists the dissociation thresholds derived via this fitting process, i.e., for the hypothetical isotopomer $^{79}Br^{35.5}Cl$. The deduced differences in threshold energy between channels 1 and 2 (881.8 cm^{-1}) and between channels 3 and 4 (879.8 cm^{-1}) agree very well (to within 1σ) with the known spin−orbit splitting in atomic chlorine (882.4 cm^{-1}). Similarly, the energetic separation of the derived thresholds for channels 1 and 5 (3137.1 cm^{-1}) is in excellent accord with the literature value (3136.4 cm^{-1}) for the $^3P_1-^3P_2$ spin−orbit splitting in the Br^+ ion. Thus the threshold energy differences between channels 1 and 3 and channels 2 and 4, should provide by far the most accurate measure of the spin−orbit splitting in the ground state of $BrCl^+$ yet reported. The error-weighted value so derived, $A = -2070.4 \pm 4$ cm^{-1} (where the minus sign is included in recognition that $BrCl^+$ has an inverted $^2\Pi$ ground state) is in perfect agreement with the earlier value of Dunlavey et al.,[18] though the precision is much improved in the present measurement. Deriving dissociation energies (D_0 values) for the $^2\Pi_{3/2}$ and $^2\Pi_{1/2}$ states requires a little more thought. The best-fit values are, respectively, 25 020.4 ± 3 cm^{-1} and 22 949.5 ± 1 cm^{-1}, but these are "effective" D_0 values for forming $^{79}Br^+$ ions from a mixture of $^{79}Br^{35}Cl^+$ and $^{79}Br^{37}Cl^+$ parent ions, the zero-point energies of which differ by some 4 cm^{-1}. Weighting by their natural abundances would suggest that the effective D_0 values should be lowered by ∼1 cm^{-1} in the case of $^{79}Br^{35}Cl^+$ and increased by ∼3 cm^{-1} for $^{79}Br^{37}Cl^+$. Thus we arrive at the values $D_0(^{79}Br^{35}Cl^+;^2\Pi_{3/2}) = 25\,019 \pm 4$ cm^{-1} and $D_0(^{79}Br^{35}Cl^+;^2\Pi_{1/2}) = 22\,949 \pm 2$ cm^{-1}. These values, in turn, offer the most precise route yet to the adiabatic ionization potentials (IPs) for forming these two spin−orbit states of $BrCl^+$. This calculation makes use of the dissociation energy of the ground-state neutral ($D_0 = 18\,026 \pm 2$ cm^{-1} derived from the reported D_e value[35] and spectroscopic constants[30] for $^{79}Br^{35}Cl$) and the documented IP for Br (95 284.8 cm^{-1}, ref 33), from which we deduce

$$\begin{aligned} &IP[BrCl(v'' = 0) \rightarrow BrCl^+(^2\Pi_{3/2}, v^+ = 0)] = \\ &\quad IP[Br \rightarrow Br^+(^3P_2)] + D_0(Br-Cl) - D_0(Br^+-Cl) = \\ &\quad 88\,292 \pm 6\ \text{cm}^{-1}\ (10.9468 \pm 0.0007\ \text{eV}) \quad (4) \end{aligned}$$

for the $^{79}Br^{35}Cl$ isotopomer. This value also agrees well with the maximum of the lowest energy peak evident in the He I photoelectron spectrum reported by Dunlavey et al.[18] We determine the corresponding IP for forming $^{79}Br^{35}Cl^+(^2\Pi_{1/2})]$ ions as 90 362 ± 4 cm^{-1} (11.2035 ± 0.0005 eV). Given $IP[Cl \rightarrow Cl^+(^3P_2)] = 104\,590.2$ cm^{-1}, we can also calculate rather precise energetic thresholds for forming ground-state $^{79}Br + {}^{35}Cl^+$ products − 122 616 ± 2 cm^{-1} from $^{79}Br^{35}Cl(X, v'' = 0)$ and 34 324 ± 6 cm^{-1} from $^{79}Br^{35}Cl^+(X^2\Pi_{3/2}, v^+=0)$.

Conclusions

High-resolution imaging studies of the Br^+ fragments resulting from photodissociation of state-selected $BrCl^+$ cations have yielded the most precise values yet reported for (i) the spin−orbit coupling constant for the $X^2\Pi$ state, $A = -2070 \pm 4$ cm^{-1}; (ii) the bond-dissociation energies of both states of $^{79}Br^{35}Cl^+$, 25 019 ± 4 cm^{-1} ($X^2\Pi_{3/2}$) and 22 949 ± 2 cm^{-1} ($X^2\Pi_{1/2}$); (iii) the adiabatic ionization thresholds for forming $^{79}Br^{35}Cl^+$ parent ions in their $X^2\Pi_{3/2}$ and $X^2\Pi_{1/2}$ states, 88 292 ± 6 cm^{-1} and 90 362 ± 4 cm^{-1}, respectively. Consideration of the measured wavelength dependence of the branching ratios for forming ground and spin−orbit excited Cl atoms following photolysis of $BrCl^+$ parent ions, as a function of spin−orbit state (i.e., product channels 1 and 2 and 3 and 4), and the recoil anisotropies of these various fragmentation channels, is reserved for a future publication.[31] So, too, is any description of corresponding studies of the Cl^+ fragment ion forming channels that appear most noticeably at shorter excitation wavelengths, and a detailed discussion of the underlying fragmentation dynamics in the context of calculated ab initio potentials for the various excited valence states of $BrCl^+$.

Acknowledgment. Funding from the Commission of the European Communities [IHP Contract No. HPRN-CT-2002-00183 (PICNIC) and MEIF-CT-2003-500999 (PHOSPHOR) for N.H.N.] is gratefully acknowledged. The Bristol group is also most grateful to the EPSRC for financial support via the pilot portfolio partnership LASER and to colleagues K. N. Rosser, R. N. Dixon, C. Murray, A. J. Orr-Ewing, and C. M. Western for their many and varied contributions to the work described herein. The work in Nijmegen is supported by the Dutch National Science Foundation NWO-CW Project Number 700.98.306.

References and Notes

(1) Chandler, D. W.; Houston, P. L. *J. Chem. Phys*. **1987**, *87*, 1445.
(2) Eppink, A. T. J. B.; Parker, D. H. *Rev. Sci. Instrum.* **1997**, *68*, 3477.
(3) Wrede, E.; Laubach, S.; Schulenburg, S.; Brown, A.; Wouters, E. R.; Orr-Ewing, A. J.; Ashfold, M. N. R. *J. Chem. Phys*. **2001**, *114*, 2629.
(4) Dylewski, S. M.; Geiser, J. D.; Houston, P. L. *J. Chem. Phys*. **2001**, *115*, 7460 and references therein.
(5) Wouters, E. R.; Beckert, M.; Russell, L. J.; Rosser, K. N.; Orr-Ewing, A. J.; Ashfold, M. N. R.; Vasyutinskii, O. S. *J. Chem. Phys*. **2002**, *117*, 2087 and references therein.
(6) Rakitzis, T. P.; Kitsopoulos, T. N. *J. Chem. Phys*. **2002**, *116*, 9228 and references therein.
(7) Brouard, M.; Clark, A. P.; Vallance, C.; Vasyutinskii, O. S. *J. Chem. Phys.* **2003**, *119*, 771.
(8) Potter, A. B.; Dribinski, V.; Demyanenko, A. V.; Reisler, H. *J. Chem. Phys*. **2003**, *119*, 7197 and references therein.
(9) Beckert, M.; Wouters, E. R.; Ashfold, M. N. R.; Wrede, E. *J. Chem. Phys*. **2003**, *119*, 9576 and references therein.
(10) Surber, E.; Sanov, A. *J. Chem. Phys.* **2002**, *116*, 5921 and references therein.
(11) Romanescu, C.; Manzhos, S.; Boldovsky, D.; Clarke, J.; Loock, H. P. *J. Chem. Phys*. **2004**, *120*, 767.
(12) *Imaging in Chemical Dynamics*; Suits, A. G., Continetti, R. E., Eds.; ACS Symposium Series 770; American Chemical Society: Washington, D.C., 2001.
(13) Wouters, E. R.; Ahmed, M.; Peterka, D. S.; Bracker, A. S.; Suits, A. G.; Vasyutinskii, O. S. *Imaging in Chemical Dynamics*; Suits, A. G., Continetti, R. E., Eds.; ACS Symposium Series 770; American Chemical Society: Washington, D.C., 2001; pp 238−84.
(14) Rakitzis, T. P.; van der Bron, A. J.; Janssen, M. H. M. *Chem. Phys. Lett.* **2003**, *372*, 187.
(15) Beckert, M.; Greaves, S. J.; Ashfold, M. N. R. *Phys. Chem. Chem. Phys.* **2003**, *5*, 308.
(16) Vieuxmaire, O. P. J.; Nix, M. G. D.; Fitzpatrick, J. A. J.; Beckert, M.; Dixon, R. N.; Ashfold, M. N. R. *Phys. Chem. Chem. Phys*. **2004**, *6*, 543.
(17) Aguirre, F.; Pratt, S. T. *J. Chem. Phys*. **2003**, *118*, 6318, 9467.
(18) Dunlavey, S. J.; Dyke, J. M.; Morris, A. *J. Electron Spectrosc. Relat. Phenom*. **1977**, *12*, 259.
(19) Hubinger, S.; Nee, J. B. *J. Photochem. Photobiol. A* **1995**, *86*, 1 and references therein.
(20) Hopkirk, A.; Shaw, D.; Donovan, R. J.; Lawley, K. P.; Yencha, A. *J. Phys. Chem*. **1989**, *93*, 7338.
(21) Chakraborty, D. K.; Tellinghuisen, P. C.; Tellinghuisen, J. *Chem. Phys. Lett.* **1987**, *141*, 36.
(22) Dimov, S. S.; Lipson, R. H.; Turgeon, T.; Vanstone, J. A.; Wang, P.; Yang, D. S. *J. Chem. Phys*. **1994**, *100*, 8666.
(23) Eppink, A. T. J. B.; Parker, D. H. *J. Chem. Phys*. **1999**, *110*, 832.
(24) Wrede, E.; Laubach, S.; Schulenburg, S.; Orr-Ewing, A. J.; Ashfold, M. N. R. *Chem. Phys. Lett*. **2000**, *326*, 22.
(25) Sato, Y.; Matsumi, Y.; Kawasaki, M.; Tsukiyama, K.; Bersohn, R. *J. Phys. Chem.* **1995**, *99* 16307.
(26) Ashfold, M. N. R.; Howe, J. D. *Annu. Rev. Phys. Chem*. **1994**, *45*, 57 and references therein.
(27) de Lange, C. A. *Adv. Chem. Phys.* **2001**, *117*, 1 and references therein.
(28) Samartzis, P. C.; Kitsopoulos, T. N.; Ashfold, M. N. R. *Phys. Chem. Chem. Phys.* **2000**, *2*, 453.
(29) Lawley, K. P.; Donovan, R. J.; Ridley, T.; Yencha, A. J.; Ichimura, T. *Chem. Phys. Lett.* **1990**, *168*, 168.
(30) Huber, K. P.; Herzberg, G. Constants of Diatomic Molecules (data prepared by Gallagher, J. W.; Johnson, R. D., III). In *NIST Chemistry WebBook*; Linstrom, P. J., Mallard, W. G., Eds.; NIST Standard Reference Database Number 69; National Institute of Standards and Technology: Gaithersburg, MD, 2003 (http://webbook.nist.gov).
(31) Vieuxmaire, O. P. J.; Nahler, N. H.; Jones, J. R.; Dixon, R. N.; Ashfold, M. N. R. Manuscript in preparation.
(32) Li, L.; Lipert, R. J.; Lobue, J.; Chupka, W. A.; Colson, S. D. *Chem. Phys. Lett*. **1988**, *151*, 335.
(33) NIST Atomic Spectra Database. http://physics.nist.gov/cgi-bin/AtData/main_asd.
(34) Press, W. H.; Teukolsky, S. A.; Vetterling, W. T.; Flannary, B. P. *Numerical Recipes in C*; Cambridge University Press: Cambridge, 1994.
(35) Tellinghuisen, J. *J. Phys. Chem. A* **2003**, *107*, 753.